Scaling up real networks by geometric branching growth

Muhua Zheng[a,b,c], Guillermo García-Pérez[d,e,f], Marián Boguñá[b,c], and M. Ángeles Serrano[b,c,g,1]

[a]School of Physics and Electronic Engineering, Jiangsu University, Zhenjiang 212013, China; [b]Departament de Física de la Matèria Condensada, Universitat de Barcelona, 08028 Barcelona, Spain; [c]Universitat de Barcelona Institute of Complex Systems, Universitat de Barcelona, 08028 Barcelona, Spain; [d]Quantum Technology Finland Centre of Excellence, Turku Centre for Quantum Physics, Department of Physics and Astronomy, University of Turku, FI-20014 Turun Yliopisto, Finland; [e]Complex Systems Research Group, Department of Mathematics and Statistics, University of Turku, FI-20014 Turun Yliopisto, Finland; [f]Algorithmiq Ltd, 20100 Turku, Finland; and [g]Catalan Institution for Research and Advanced Studies (ICREA), 08010 Barcelona, Spain

Edited by Sune Lehmann, Technical University of Denmark, Kongens Lyngby, Denmark, and accepted by Editorial Board Member David L. Donoho April 6, 2021 (received for review September 15, 2020)

Real networks often grow through the sequential addition of new nodes that connect to older ones in the graph. However, many real systems evolve through the branching of fundamental units, whether those be scientific fields, countries, or species. Here, we provide empirical evidence for self-similar growth of network structure in the evolution of real systems—the journal-citation network and the world trade web—and present the geometric branching growth model, which predicts this evolution and explains the symmetries observed. The model produces multiscale unfolding of a network in a sequence of scaled-up replicas preserving network features, including clustering and community structure, at all scales. Practical applications in real instances include the tuning of network size for best response to external influence and finite-size scaling to assess critical behavior under random link failures.

complex network | self-similarity | network evolution | geometric branching growth | geometric renormalization

In the context of network science, growth is most often modeled through the sequential addition of new nodes that connect to older ones in a graph by different attachment mechanisms (1, 2), including models of hidden variables, where nodes are characterized by intrinsic properties (3, 4). Other growth processes have also been considered, such as duplication to explain large-scale proteome evolution (5, 6). Here, we take an alternative approach and explore the relation between branching growth (7) and geometric renormalization (GR) (8) to explain self-similar network evolution. Renormalization in networks, based on the ideas of the renormalization group in statistical physics (9–11), acts as a sort of inverse branching process by coarse-graining nodes and rescaling interactions. Thus, branching growth can be seen as an inverse renormalization transformation: an idea that was introduced in ref. 12 using a purely topological approach to reproduce the structure of fractal networks, where fractality was interpreted as an evolutionary drive toward robustness. However, topological distances in networks are seriously constrained by the small-world property, while the characterization of fractality in real networks disregards fundamental features of their structure, including clustering and community organization.

GR (8) is an alternative technique that can be performed by virtue of the discovery that the structure of real networks is underlain by a latent hyperbolic geometry (13, 14). Thus, the likelihood of interactions between nodes depends on their distances in the underlying space, via a universal connectivity law that operates at all scales and simultaneously encodes short- and long-range connections. This approach has been able to explain many features of the structure of real networks, including the small-world property, scale-free degree distributions, and clustering, as well as fundamental mechanisms such as preferential attachment in growing networks (4) and the emergence of communities (15, 16). Given a network map, GR produces a multiscale unfolding of the network in scaled-down replicas over progressively longer length scales. This transformation has revealed self-similarity to be a ubiquitous symmetry in real networks, whose structural properties remain scale-invariant as the observational resolution is decreased (8). This poses the question of whether this self-similarity could be related to the mechanisms driving the growth of real networks and, therefore, whether their evolution could be conceptualized within the framework of the GR group.

In this work, we show that real networks—citations between scientific journals (17, 18) and international trade (19)—have evolved in a self-similar way over time spans of more than 100 y, meaning that their local, mesoscale, and global topological properties remain in a steady state as time goes by, with a moderate increase of the average degree. We demonstrate that the observations can be modeled by a geometric branching growth (GBG) process that produces a self-similar metric expansion. Beyond the capacity of the model to explain and predict the self-similar evolution of real networks effectively, the technique is flexible and allows us to generate scaled-up network replicas that, when combined with scaled-down network replicas (8), provide a full up-and-down self-similar multiscale unfolding of complex networks that covers both large and small scales. We illustrate the use of GBG multiscale unfolding in real network instances via the tuning of network size for optimal response to

Significance

Branching processes underpin the complex evolution of many real systems. However, network models typically describe network growth in terms of a sequential addition of nodes. Here, we measured the evolution of real networks—journal citations and international trade—over a 100-y period and found that they grow in a self-similar way that preserves their structural features over time. This observation can be explained by a geometric branching growth model that generates a multiscale unfolding of the network by using a combination of branching growth and a hidden metric space approach. Our model enables multiple practical applications, including the detection of optimal network size for maximal response to an external influence and a finite-size scaling analysis of critical behavior.

Author contributions: M.Á.S. designed research; M.Z., G.G.-P., M.B., and M.Á.S. performed research; M.Z., G.G.-P., M.B., and M.Á.S. analyzed data; and M.Z., G.G.-P., M.B., and M.Á.S. wrote the paper.

The authors declare no competing interest.

This article is a PNAS Direct Submission. S.L. is a guest editor invited by the Editorial Board.

[1]To whom correspondence may be addressed. Email: marian.serrano@ub.edu.

This article contains supporting information online at https://www.pnas.org/lookup/suppl/doi:10.1073/pnas.2018994118/-/DCSupplemental.

Published May 18, 2021.

an external influence, referred to here as "the optimal mass," and a finite-size scaling analysis of critical behavior under random link failures.

Self-Similar Evolution of Real Networks

We consider the evolution of the journal-citation network (JCN) (17) and of the world trade web (WTW) (19) over time spans of more than 100 years.

The evolution of JCNs offers a quantitative proxy for the development of contemporary science and the emergence of a vast number of new scientific fields and subfields, driven by diversification and specialization (17, 18, 20–22). Here, we analyze data from ref. 17, where the time period 1900–2013 is divided into time windows of 10 y before 1970 and of 5 y thereafter. One citation network is reconstructed for each time window, where journals are represented as nodes that are linked whenever citations between their publications exist.

An increase of the number of actors is also a hallmark of the evolution of the international trade system. The number of sovereign states in the world increased from 42 in 1900 to 195 in 2016 (23), mainly due to processes such as decolonization; the dismantlement of large or multicultural states such as the USSR and Yugoslavia (1991) into a number of smaller states; the parliamentary split of an existing state into two, as happened in Czechoslovakia (1993); and independence processes after civil wars, like that of the Republic of South Sudan and the Republic of the Sudan (2011). Here, we use networks in the World Trade Atlas (19), a collection of annual world trade network maps in hyperbolic geometry, which provide information on the long-term evolution of the international trade system from 1870 to 2013, where nodes represent countries linked by bilateral trade relationships. The maps revealed that globalization, hierarchization, and localization are main forces shaping the trade space, which naturally exhibits hyperbolic geometry, rather than Euclidean, as a reflection of its complex architecture.

More details of the two datasets are available in *SI Appendix*, section I, and the main statistical properties are in *SI Appendix*, Tables S1 and S2.

The size N of the two evolving networks increases over time, ranging from 118 journals in 1900–1910 to 21,460 in 2008–2013 and from 24 countries in 1870 to 189 in 2013 (*SI Appendix*, Fig. S1 *A* and *B*). After World War II, the average degree $\langle k \rangle$ only shows a moderate increase in the JCN and almost flat behavior in the WTW (*SI Appendix*, Fig. S1 *C* and *D*). Degree distributions, clustering spectra, degree–degree correlations, and the community structure of some snapshots are shown for the JCN in Fig. 1 and for the WTW in *SI Appendix*, Fig. S2 (results for all snapshots are in *SI Appendix*, Figs. S3–S5). We observe clear-cut self-similar behavior with the curves for different networks overlapping when the degrees of the nodes are rescaled by the average degree of the corresponding network. Fig. 1*D* and *SI Appendix*, Fig. S2D show the modularity, Q, of the optimal partitions of the nodes into different communities detected by the Louvain method (24) and the adjusted mutual information, AMI (25), between the optimal partitions of two consecutive snapshots, in which we only considered the nodes that exist in both. The level of modularity remains stable throughout the evolution of the systems and the overlap between communities in the consecutive snapshots is consistently very high. This indicates that the community structure is mostly preserved as time goes by. Hence, the empirical evidence presented so far indicates that these real networks grow in a self-similar fashion.

GBG

The key property that characterizes the evolution of the systems under study is inheritance. Indeed, when a scientific field gives rise to the birth of new subfields, the offspring will inherit thematic topics similar to those of the parent field. Likewise, when a country breaks up, the new sovereign countries will inherit the wealth and trade partners of the original state. In network

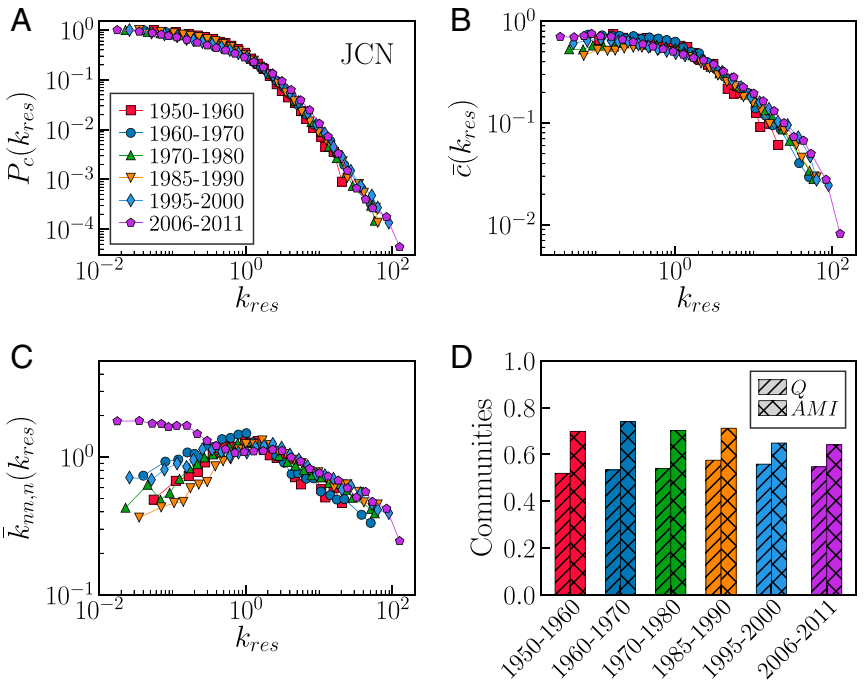

Fig. 1. Self-similar evolution of real networks. (*A*) Complementary cumulative distribution $P_c(k_{res})$ of rescaled degrees $k_{res} = k/\langle k \rangle$ for different time snapshots in the JCN. (*B*) Degree-dependent clustering coefficient $\bar{c}(k_{res})$ over rescaled-degree classes. (*C*) Degree–degree correlations, as measured by the normalized average nearest-neighbor degree $\bar{k}_{nn,n}(k_{res}) = \bar{k}_{nn}(k_{res})\langle k \rangle / \langle k^2 \rangle$. (*D*) Modularity, Q, and adjusted mutual information, AMI, between the community partitions of two consecutive snapshots by considering nodes existing in snapshots in the JCN. A few representative snapshots are shown here. Results for all networks in the period analyzed are in *SI Appendix*, Figs. S3–S5.

terms, this means that when a node belonging to a given community splits, offspring nodes most likely will belong to the same community establishing relations preferentially with similar partners. In addition, the degree of a node can be considered as a proxy of its wealth. Thus, when a node splits, we expect that its ability to generate connections will be partially inherited by the newborn offspring. Following these principles, we introduce a model for network evolution that is able to incorporate inheritance while preserving the self-similarity observed in real systems.

The model is based on a geometric description of networks that provides a simple and accurate explanation for the observed regularities in real systems (26). Such representation assigns two coordinates to every node in a real network, one related to its similarity to other nodes and another to its degree (13), so it seems particularly suited for our problem. The combination of the two components leads to hyperbolic space as the natural geometry underlying the hierarchical architecture of networks (27). The GBG mechanism that we propose here splits existing nodes into offspring that are placed in a close neighborhood of their parent's node location in the underlying space. In this way, newborn nodes automatically inherit structural properties of their parent node effectively encoded in the similarity and popularity coordinates that determine their connections in the evolved network. By iterative application, the GBG transformation produces, thus, a self-similar multiscale unfolding of the network in a shell of scaled-up replicas of progressively increasing size. This mechanism is illustrated in Fig. 2*A*, where the similarity subspace is represented as a circle, and the size of the node is related to its degree. In the next subsection, we briefly explain the basics of the geometric description of networks before introducing the GBG model.

Geometric Description of Complex Networks. The GBG model introduced in this work is built upon a geometric description of complex networks, which is very well described by the $\mathbb{S}^1$ model (13). The $\mathbb{S}^1$ model is a hidden-variables model, meaning that nodes are assigned attributes that modulate the likelihood of

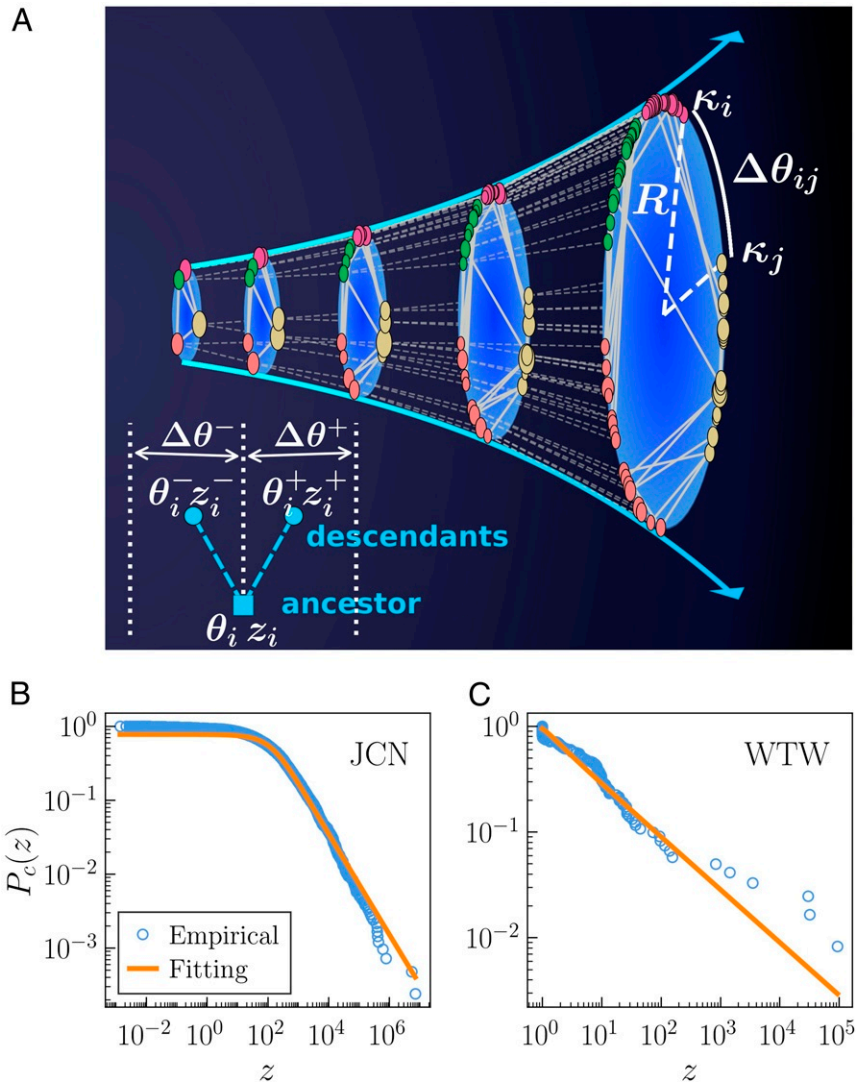

Fig. 2. Sketch of the GBG model. (*A*) In each layer of the self-similar upwards multiscale unfolding, the size of each node is proportional to the logarithm of its hidden degree, κ. Different colors represent different geometric communities. Dashed lines connect ancestors to their descendants along the flow (blue arrows). A pair of nodes, i and j, with hidden degrees κ_i and κ_j has been highlighted, for which the angular separation, $\Delta\theta_{ij}$, represents their similarity distance. In *A*, *Inset*, we show a sketch of the branching process from an ancestor to its pair of descendants. The complementary cumulative distribution of z values together with their corresponding stable distribution fittings are in *B* for JCN 1965–1975 and in *C* for WTW 1965.

connections. More specifically, each node i is assigned a hidden degree κ_i that measures its popularity—wealth, influence, ...–, and an angular position θ_i in a one-dimensional sphere (or circle) representing the similarity space. The hidden degree of node i sets its scale of connectivity and gives the ensemble average degree of the node—that is, if node i has hidden degree κ_i, then its expected degree is $\bar{k}(\kappa_i)=\kappa_i$, where the bar denotes the ensemble average over many network realizations. Every pair of nodes, i and j, is connected with probability

$$p_{ij}=\frac{1}{1+\chi_{ij}^{\beta}}=\frac{1}{1+\left(\frac{R\Delta\theta_{ij}}{\mu\kappa_i\kappa_j}\right)^{\beta}}, \qquad [1]$$

that takes a gravity law form so that more popular (larger κ) or more similar (lower $\Delta\theta$) nodes are more likely to form connections (13). The similarity circle has radius R adjusted to maintain a constant density of nodes equal to one, without loss of generality. The model has two main parameters: $\beta>1$, controlling the average clustering coefficient $\langle c\rangle$, and μ, adjusting the network average degree $\langle k\rangle$. Degree heterogeneity is controlled by the distribution of hidden degrees, and community structure is encoded into the angular distribution of nodes in the similarity space.

Interestingly, the $\mathbb{S}^1$ model is equivalent, through an isomorphism, to another geometric model, the $\mathbb{H}^2$ model (27). The isomorphism maps the hidden degree κ_i to a radial coordinate, $r_i=R_{\mathbb{H}^2}-2\ln\frac{\kappa_i}{\kappa_0}$, while keeping the same angular position. Upon this transformation, each node is positioned in a point of the hyperbolic plane (r_i,θ_i), while the connection probability (Eq. **1**) becomes a function of the hyperbolic distance among nodes only (27). Hyperbolic distances are then measured with the metric tensor $ds^2=dr^2+\sinh^2 rd\theta^2$. Both the $\mathbb{S}^1$ and $\mathbb{H}^2$ models are different faces of the same coin, as they generate the same ensemble of networks. In a certain sense, this equivalence is similar to the equivalence between Newton's view of gravity as an interaction due to the mass of bodies and Einstein's perspective, where gravity is just a geometric effect due to the deformation of spacetime. Each formulation can be used depending on the particular application. For instance, the $\mathbb{H}^2$ is more suitable for navigability (28), whereas the $\mathbb{S}^1$ is more convenient for community detection (19). Notice that in contrast to $\mathbb{H}^2$, each hidden variable in $\mathbb{S}^1$ has an explicit contribution to the probability of connection. Such explicit contributions turn out to be crucial for our GBG model.

The clue for the connection between topology and geometry in the $\mathbb{S}^1/\mathbb{H}^2$ model is clustering, which arises as a reflection of the triangle inequality in the underlying space. Notice that clustering in a network is a form of many-body interactions among nodes, so that any model aiming at reproducing clustering must include these effects either directly or effectively. When interactions are pairwise, geometry induces in a natural way effective many-body interactions and so clustering. Among all geometric random graphs models, the $\mathbb{S}^1$ model is able to reproduce sparse, small-world, highly clustered networks with heterogeneous degree distributions using a single connectivity law that encodes short- and long-range connections simultaneously. The model is able to do so while being a maximum-entropy model, meaning that the model makes the minimum number of assumptions to explain observations (29), so it is the most parsimonious option. Likewise, the $\mathbb{S}^1/\mathbb{H}^2$ model is particularly interesting because a body of analytic results for the most relevant topological properties have already been derived, including degree distribution (13, 27, 30), clustering (27, 30, 31), diameter (32–34), percolation (35, 36), self-similarity (13), or spectral properties (37). The model has been extended to weighted networks (38) and multiplexes (39–41) and has been used to model real networks from many different domains, from metabolic networks (42) or the brain (43, 44) to the WTW (19) and the Internet (28).

Hidden degrees and angular positions of nodes in real networks (together with the parameters β and μ) can be estimated by using the tool Mercator (45) that takes as input the network topology and maximizes the probability that such structure is generated as an instance of the $\mathbb{S}^1$ model; more details can be found in *SI Appendix*, section II. The estimated values define a geometric map of the network and, due to the aforementioned isomorphism between $\mathbb{S}^1$ and $\mathbb{H}^2$, the underlying geometry is the hyperbolic plane (28). Notice that the inferred hidden degree of a node corresponds, as a first approximation, to the observed degree of the node in the real network (28), while the distribution of inferred similarity coordinates is typically inhomogeneous, so that nodes concentrate in specific regions of the circle, forming geometric communities (19, 28, 42).

The GBG Model. The GBG dynamics is inspired by the GR group introduced in ref. 8. In brief, the GR transformation (8) is applied to network maps and proceeds by defining nonoverlapping blocks of consecutive nodes of equal size r around the similarity circle, which are then coarse-grained into a single node in the renormalized lower-resolution map, where pairs of nodes are connected with a link if any of their precursor nodes were connected in the original layer. As a result, a multiscale unfolding of self-similar scaled-down network replicas is obtained, except for the average degree of the renormalized layers, which typically grows exponentially in real networks (more details are in *SI Appendix*).

Unlike GR, GBG works in the opposite direction by splitting nodes instead of merging them. The GBG transformation can be controlled to adjust the growth in the number of nodes and also the flow of the average degree, embodying a family of models that includes noninflationary and inflationary growth. Noninflationary growth produces a sequence of progressively magnified layers with decreasing average degree that comply with GR, meaning that when GR is applied to the layer obtained after the GBG transformation, the result is the original network. Inflationary growth means that scaled-up shell layers are produced with an average degree that does not decrease very fast, or even increases. This case is relevant to model the growth of connection over time in the JCN and the WTW.

The first step to generate a GBG scaled-up layer of a real network is to split every node in the original map into r descendants with probability p, so that the population increases as $N'=N(1+p(r-1))=bN$ with branching rate b. For mathematical convenience, we will continue the description with $r=2$ $(b=1+p)$. We can use parameter b in combination with the number of layers in the multiscale unfolding to adjust the growth of the number of nodes over the evolution of the network. Every branching node produces a pair of descendants that require the assignment of similarity coordinates in the $\mathbb{S}^1$ circle and of hidden degrees, whereas nodes that do not split remain with the same coordinates. The radius of the circle is rescaled as $R'=bR$, so that the density of nodes remains equal to one.

Assigning coordinates to descendants. One of the requirements for self-similar growth is the preservation of the ordering of nodes in the circle and their concentration across specific angular sectors defining geometric communities (15, 16). To this end, the simplest means to model growth is to place the descendants at angular coordinates θ_i^+ and θ_i^- to the left and right of the angular position of their corresponding ancestor, i, with uniform probability within a small angular separation $\Delta\theta^{\pm}$. The values $\Delta\theta^{\pm}$ are bounded by the total number of nodes in the descendant layer and by the proximity (to the left or right) of consecutive nodes to the ancestor in the similarity circle.

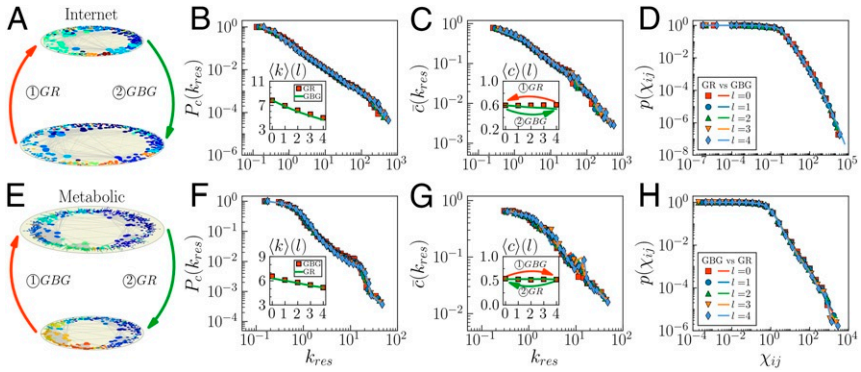

Fig. 3. GBG is compliant with GR in the noninflationary limit. (*A–D*) GR-GBG transformation in the Internet. We first renormalized the original network, applying GR four times to obtain a sequence of four layers of decreasing size. Then, we took the last layer as the original network, going back from layer 4 to layer 0 by applying GBG four consecutive times to obtain a new sequence of four layers of increasing size. Sketch *A* represents this process, from the original Internet to its renormalized version using GR (indicated by the red arrow) and then back to the reconstructed Internet using GBG (as indicated by the green arrow). Colors of nodes in *A* indicate community structure, as detected by the Louvain algorithm. Notice that both sequences of networks have the same sizes at each layer, so that they can be directly compared. *B–D* show different topological properties for the GR (symbols) and GBG (solid lines) layers. (*B*) Flow of the complementary cumulative degree distribution and, in *Inset*, the average degree that, as expected, increases during the GR phase and decreases during the GBG phase. (*C*) Flow of the degree-dependent clustering coefficient and, in *Inset*, the average clustering, which remains constant as expected. (*D*) Flow of the connection probability $p(\chi_{ij})$ as a function of the effective distance χ_{ij} in layer *l*. (*E–H*) GBG-GR transformation in the human metabolic network. In this case, the experiment was performed in the opposite order. The original network was first transformed by applying GBG to produce four layers, and then GR was applied to layer 4 to go back to layer 0. In both experiments, the branching ratio was set to $b = 1.2$.

We set $\Delta\theta^{\pm} = \min\{\frac{2\pi}{N}, \frac{\Delta\theta_{ij}}{2}\}$, where $\Delta\theta_{ij} = \pi - |\pi - |\theta_i - \theta_j||$ is the angular distance between the branching node i and its consecutive neighboring node j (to the left or right) in the ancestor layer. This choice of $\Delta\theta^{\pm}$ ensures the preservation of large gaps between consecutive nodes by limiting the angular distance between branching node and descendant, while it prevents crossings between descendants of neighboring branching nodes, even in densely populated angular regions. In this way, the community organization encoded in the angular distribution of nodes is inherited from the old layer to the new one.

To assign the hidden degrees κ^+ and κ^-, we impose two conditions. First, the hidden degrees of ancestors and descendants need to comply with GR. In ref. 8, it was shown that the quantity $z = \kappa^{\beta}$ is conserved by GR when two nodes are merged into a supernode. Therefore, we now demand that whenever a node with wealth z splits into two, its wealth z is conserved and inherited by the two offspring, so that $z = z^+ + z^-$. Second, the hidden degrees of descendants must be independent and identically distributed (iid) random variables with a distribution of hidden degrees that preserves that of the ancestor layer, $\rho(\kappa)$ [equivalently, $\rho(z)$]. Taking the two conditions together, the transformed hidden degrees $z^{\pm}$ of descendants should satisfy:

$$\iint \mathrm{d}z^+ \mathrm{d}z^- \rho(z^+)\rho(z^-)\delta\left(z - \left(z^+ + z^-\right)\right) = \rho(z). \qquad [2]$$

The equation above implies that $\rho(z)$ is a stable distribution (46–48), meaning that the linear combination of two independent variables with probability distribution $\rho(z)$ has the same distribution, up to scaling and location factors. Stable distributions admit multiple parametrizations, but are always defined by four parameters $f(z;\alpha,\eta,c,d)$: the tail exponent $\alpha \in (0,2]$ and skewness $\eta \in [-1,1]$, which control the shape; and c and d for scale and location (*SI Appendix*, section III). Stable distributions conform a rich family of models, including Gaussian ($\alpha = 2$), Cauchy ($\alpha = 1$ and $\eta = 0$), Lévy ($\alpha = 1/2$ and $\eta = 1$), and Landau ($\alpha = 1$ and $\eta = 1$) distributions. Stable distributions are infinitely divisible and are the only possible limit distributions for properly normalized and centered sums of iid random variables (generalized Central Limit Theorem) (49). In addition, they can accommodate fat tails and asymmetry and, therefore, often offer a very good fit for empirical data (48, 50–52). Fig. 2 *B* and *C* show very good fits for the JCN and WTW in the original layers (53, 54) (see *SI Appendix*, Fig. S6 for more empirical networks and the corresponding fitting parameters in *SI Appendix*, Table S3). Once the parameters of the stable distribution are estimated* , we proceed to generate values of $z^{\pm}$ for descendant nodes, as described in *Materials and Methods*.

Connecting nodes in the descendant layer. Once coordinates have been assigned to offspring nodes, connections between descendants in the new layer are implemented such that the resulting network belongs to the $\mathbb{S}^1$ ensemble. In what we call the "noninflationary" limit, we also require that the new network is compliant with GR—that is, GR applied to the descendant layer should result in the ancestor layer. This implies that, in this limit, there are only connections in the descendant layer between descendants of the same ancestor or of connected ancestors. We then use the probability of connection p_{ij} Eq. **1** as in the $\mathbb{S}^1$ model, rescaling $\mu' = b\mu$ in the new layer to control the flow of the average degree and with β remaining invariant as in the GR transformation. With this probability $p_{ij}(\mu')$, we connect descendants branching from the same ancestor, and, for every pair of connected ancestors, we establish potential links among their descendants with the same probability $p_{ij}(\mu')$, but making sure that at least one link is formed between them (*SI Appendix*, section V). Finally, in the "inflationary" limit, once the previous step is accomplished, we rescale $\mu' \to a\mu'$ with $a > 1$ and add extra links in an unbiased way to match the target average degree, as described in *Materials and Methods*.

GBG Is a Statistical Inverse of GR. We support this claim with the results shown in Fig. 3 and *SI Appendix*, Figs. S7–S14 for different real networks and branching rates b, which show that the results are robust. In Fig. 3 *A–D*, we show that after applying GR to the Internet, the original network can be recovered with high fidelity (in a statistical sense) by applying the noninflationary GBG to the renormalized layer. Conversely, if we first apply the noninflationary GBG technique to obtain the scaled-up network and then

*Notice that since $\{z_i\}$ are bounded from the left, $\eta = 1$ and $\alpha < 1$.

recover the networks by GR, the result is analogous; see Fig. 3 *E–H* for the Metabolic network (details of the datasets are in *SI Appendix*, section I)[†] . This means that noninflationary GBG and GR flows produce the same values of average clustering, average degree, and empirical connection probability, among other properties. The GBG transformation also preserves the original community structure, as detected by the Louvain algorithm (24). Furthermore, since the transformation also preserves the correlation between hidden angles and degrees, the self-similarity of the scaled-up networks extends to structural correlations among nodes, such as degree–degree correlations (45).

As shown, GBG is a statistical inverse of GR, but inflationary GBG is not because of the new links added to increase the average degree over the value given by inverse GR. During the evolution of the real systems analyzed in this work, we observe a global increase of the density of connections (*SI Appendix*, Fig. S1). In the WTW, this is due to the global growth of the world gross domestic product and in the JCN to the increasing number of researchers, and thus publications, within the scientific system. Parameter a in the inflationary limit of GBG can be adjusted to model such global increase by controlling the growth of the average degree. If we apply GR to the obtained replica, we would recover an inflated version of the original network with extra links that we would need to deflate to recover the original network. To rebalance the average degree one needs an extra mechanism, like the pruning used in ref. 8 to produce scaled-down network replicas. The deflation procedure is analogous to the inflation technique, and we give the details in *SI Appendix*, sections VII and VIII. Given that the addition of links in the inflationary step of the inflationary GBG process, as well as the pruning of links to decrease the average degree of GR layers are compliant with the $\mathbb{S}^1$ model, we say then that GBG is a statistical inverse of GR, while inflationary GBG (GBG + addition of links) is a statistical inverse of deflationary GR (GR + pruning of links) (*SI Appendix*, Fig. S18).

Behavior of the Average Degree. In the noninflationary GBG model ($a=1$), we can use the inverse of the GR relation between the average degrees in a descendant layer and in the ancestor layer (8), using $\mu'=b\mu$ to obtain $\langle k\rangle^{(l)}=(b^{-\nu})^l\langle k\rangle^{(0)}$, where the scaling factor ν depends on the connectivity structure of the original network, and $\langle k\rangle^{(l)}$ (the mean degree of layer l) refers to the original network when $l=0$. Typically, as the scaling factor ν is positive in real networks (8), the average degree of the descendant layers decreases exponentially with the number of layers.

As explained previously, in the inflationary regime, μ' is rescaled by $\alpha>1$, resulting in $\mu'=ab\mu$. In this case, the average degree, $\langle k\rangle_a^{(l)}$, thus depends on a. Its behavior as a function of the network size across layers can be calculated following the same derivations as in ref. 8, which gives

$$\langle k\rangle_a^{(l)}=a^l\langle k\rangle^{(l)}=(ab^{-\nu})^l\langle k\rangle^{(0)}=\left[\frac{N^{(l)}}{N^{(0)}}\right]^{-\nu+\frac{\ln a}{\ln b}}\langle k\rangle^{(0)}, \quad [3]$$

with $N^{(l)}$ and $N^{(0)}$ the network sizes on layers l and 0, respectively.[‡] In the last step, we have used $l=\ln\left(N^{(l)}/N^{(0)}\right)/\ln b$, implied by the relation $N^{(l)}=b^lN^{(0)}$. From Eq. **3**, the average degree $\langle k\rangle_a^{(l)}$ increases as a power of $N^{(l)}$. *SI Appendix*, Fig. S19 shows the high degree of congruency between this theoretical prediction, the empirical data, and simulations (as explained below) of the inflationary version of GBG, in JCN and WTW.

Predicting the evolution of real networks. The inflationary GBG model reproduces the self-similar evolution of JCN and WTW. To support this claim, we divide the empirical data into two consecutive time windows: the first for estimation purposes and the second for validation purposes. Note that JCN and WTW data from before World War II are not used due to the high fluctuations of the network properties (*SI Appendix*, Figs. S3 and S4). We fix a value of b in the range $1<b<2$ to adjust the rate of growth in our GBG simulation in such a way that we can produce enough snapshots to compare with the real data. With this value of b, we estimate parameter a from the empirical evolution of the average degree vs. network size (see details in *SI Appendix*, section VI). We find that a remains stable over time (*SI Appendix*, Fig. S20), consistent with the empirical observation that the average degree grows as a power of the system size (Fig. 4*A* and *SI Appendix*, Fig. S21*A*). Next, we use the network snapshot at the end of the estimation period as the initial layer in GBG multiscale unfolding to simulate a number of scaled-up layers that we then compare to empirical snapshots of approximately the same size in the validation set. The comparisons of degree distributions, clustering, degree–degree correlations, and modularity are shown in Fig. 4 *D–G*. Similar results are found for the WTW (*SI Appendix*, Fig. S21).

We also measured the local rich-club and nested self-similarity effects, reported in Fig. 4*B* and *SI Appendix*, Figs. S22 and S23. We name as "local rich-club effect" and "nested self-similarity effect" the observation in real networks that the nested hierarchy of subgraphs produced by progressively thresholding the degrees of the nodes presents, respectively, an increasing internal average degree and self-similar structure (13, 35). This is a highly nontrivial property with crucial implications, such as the absence of a critical threshold in any phase transition whose critical point depends monotonously on the average degree, including percolation, epidemic spreading processes, and the Ising model (55). The results show that all of the networks analyzed in this paper, including JCN and WTW, present the two effects (*SI Appendix*, Figs. S22 and S23). Notice that standard growing network models, including the Barabási–Albert model (1) and the Popularity–Similarity Optimization model in hyperbolic space (4), have a constant average degree as the network grows, and they also present a constant average degree of the subgraphs in the nested hierarchy (*SI Appendix*, Fig. S24). Therefore, they lack the local rich-club effect. In fact, if those models were adjusted to increase the average degree over time, as happens in the real networks that we analyze in this work, the flow of the average degree in the nested hierarchy would be decreasing, in stark contrast to the empirical observations (*SI Appendix*, Fig. S24*B*). In addition, the results are robust for different values of b and for different starting times (*SI Appendix*, Fig. S25–S27). Therefore, the GBG model reproduces the self-similar evolution of the structure of the two networks with high fidelity. More comparisons between the model and empirical observations are also shown in *SI Appendix*, Figs. S28–S31.

Scaled-Up Real Network Replicas

The GBG model is not only able to explain the self-similar growth of real networks, but it can also be used as a technique to produce magnified replicas of real networks in research scenarios very different from the study of network evolution. Scaled-up replicas of real networks are versions where the number of nodes

[†]Notice that the semigroup property of GR also holds for GBG, meaning that two consecutive GBG transformations of scale b over a network are equivalent to a single transformation of scale b^2. This is easy to derive when the branching rate has an integer value, but it holds even if $b<2$. Results supporting this claim are shown in *SI Appendix*, Fig. S15 for a synthetic network produced with the $\mathbb{S}^1$ model and different values of b and in *SI Appendix*, Figs. S16 and S17 for different real networks.

[‡]Notice that the inflationary process is applied here to every layer in the flow. If, instead, it is applied in a single step to the last layer produced in a noninflationary GBG transformation, then $\langle k\rangle_a^{(l)}=a\langle k\rangle^{(l)}=a(b^{-\nu})^l\langle k\rangle^{(0)}$.

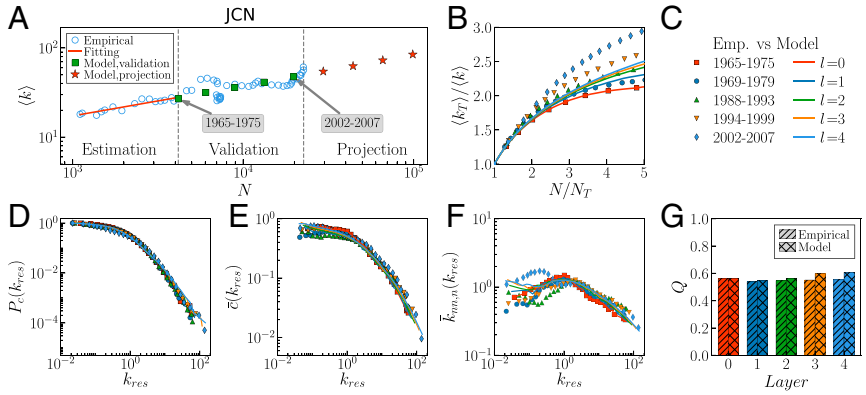

Fig. 4. The GBG model predicts the self-similar evolution of real networks. (*A*) Evolution of the average degree $\langle k \rangle$ vs. network size N. The estimation, validation, and projection sections are separated by vertical dashed lines. Blue circles, green squares, and red stars represent empirical data, validation points, and projection from the model, respectively. The data in the estimation section are used to find values of a (see details in *SI Appendix*, section VI). The branching rate, b, is fixed to 1.5, and the corresponding value of a is 1.415 (*SI Appendix*, Fig. S20). For validation purposes, we grow the network from 1965 to 1975 using GBG and compare the resulting networks with empirical (Emp.) snapshots of the same size. The equivalence between given snapshots of the real JCN and the networks generated by GBG is stated in *C*. In *D*–*G*, we show a comparison of the topological properties of simulated and empirical networks. (*B*) Local rich-club effect. (*D*) Complementary cumulative distribution of rescaled degrees. (*E*) Degree-dependent clustering coefficient over rescaled-degree classes. (*F*) Degree–degree correlations. (*G*) The modularity Q.

is increased while preserving the statistical properties of the original network, in particular, its average degree $\langle k^{(0)} \rangle$. Using GBG, the procedure is straightforward and involves adjusting the parameter b, the number of layers l, and the inflationary parameter a. The idea is to single out a specific scale after a certain number of noninflationary GBG steps and to tune a to increase the average degree to the target value by adding new links using Eq. **5** (see details in *SI Appendix*, section VII). Notice that this application of the GBG model can also be extended to networks that do not necessarily evolve according to the model, as it exploits the underlying geometric structure and congruency with geometric models observed in many real-world networks.

More specifically, GBG, possibly in combination with GR, allows us to investigate size effects in real networks, a prospect that becomes extremely useful in different applications. We illustrate this through two examples. In the first, we explore a dynamical model of opinion formation running on a real network—a Facebook network—with the goal of detecting the network size that produces an optimal response of the system to an external influence. In the second, we combine scale-up network replicas produced by GBG with scaled-down network replicas produced by GR (as described in ref. 8) to explore the critical behavior of a real network, the Internet, close to the transition where the global connectivity of the network disintegrates under random link failures.

Size-induced stochastic resonance in real networks.

We study the behavior of a model of opinion formation that depends nontrivially on the size of the network on which it runs. Here, we use a small Facebook network of 320 users working for the same software company (56) (see data description in *SI Appendix*, section I). The opinion-formation model was introduced in ref. 57. The opinion of a node can change due to imitation following a majority rule, an external influence in the form of a periodic "fashion" wave, or noise. This model was shown to present a stochastic resonance effect in small-world networks (58), displaying an optimal response of the population to the fashion wave for some noise level. The system also displays a size-induced stochastic resonance effect (59, 60), which means there is an optimal value for the number of nodes, the optimal mass, for which the average opinion best follows the fashion, as a consequence of the coupling between noise and system size.

However, those results were for graphs produced by network models that allow one to control the size of the generated networks, and not for real networks. The GBG technique provides the opportunity to study size-induced stochastic resonance in real networks. We produced a GBG self-similar multiscale shell of the Facebook network preserving the average degree of the original network (see *SI Appendix*, Fig. S32 for the statistical properties of the replicas as compared with the original network) and simulated the dynamical process described next in each layer. Each node has one of two possible opinions. At each time step of the process, a node is randomly selected and goes through a sequence of operations. The node first adopts the majority opinion among its connected neighbors, then it is forced to follow the fashion with a probability that depends on the strength and periodicity of the fashion, and, finally, it adopts randomly a new opinion with a probability that depends on the intensity of the random noise (see *SI Appendix*, section IX for details of our implementation). We modeled the external influence as a cosine function with amplitude A and period T and measured the response of the system as a function of the noise intensity ϵ for different system sizes. To measure the response of the system, we used the spectral amplification factor (61) $R = 4A^{-2}|\langle e^{i2\pi t/T}\rho(t)\rangle|$, where $\rho(t) = \frac{1}{N}\sum_i m_i(t)$ is the average opinion in the evolution, $m_i(t)$ is the opinion of node i at time t, and $\langle \cdots \rangle$ denotes a time average.

The results are shown in Fig. 5*A*. The optimal response, $R_{\max}$, is plotted in *Inset* as a function of N. For each size, N, there is a maximum response for some intermediate value of the noise and the optimal value occurs at some combination of noise and size. Interestingly, for sufficiently small values of noise (Fig. 5*C*), R is enhanced by increasing the noise, and for every noise intensity, ϵ, the optimal response occurs at approximately the same value as in $R_{\max}$, $N = 2{,}379$. Hence, we conclude that there is an optimal mass for which the average opinion best follows the external influence. Moreover, we also found that there is some value of N for which R has a minimum—that is, the average opinion follows the external influence to the least extent.

Critical behavior of real networks under random link failures.

The random failure of links in networks leads to a percolation transition: a continuous structural change that disaggregates the large cluster of connected network nodes into a bundle of small isolated components (35, 55), hence disabling the system.

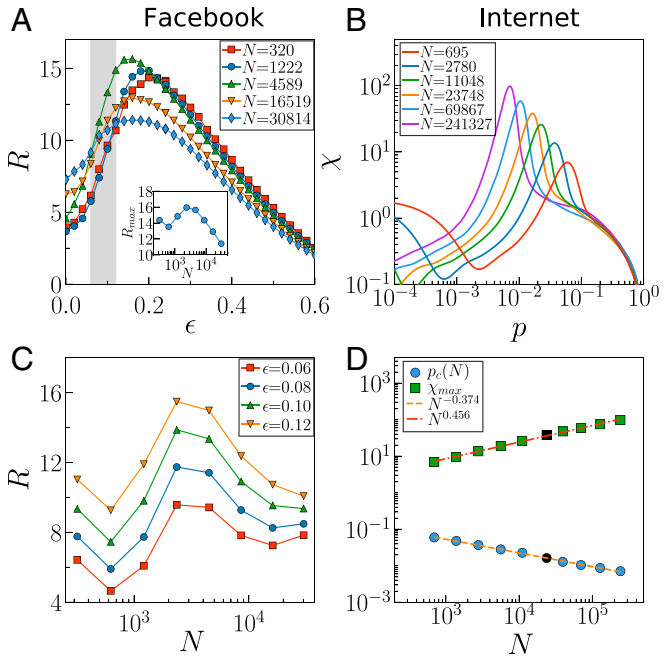

Fig. 5. Controlling network size from network snapshots. (*A* and *C*) Optimal mass of a Facebook network for best response to external modulation in a noisy environment. (*A*) System response, *R*, as a function of the noise intensity, ϵ, for different network sizes. *A*, *Inset* shows the maximum response as a function of *N*. (*C*) System response, *R*, as a function of *N* for different values of the noise intensity, ϵ. The range of noise values on the *x* axis corresponds to the gray region in *A*. (*B* and *D*) Scaling with system size of random link failure as a bond percolation process in the Internet. (*B*) Susceptibility, χ, as a function of bond occupation probability, *p*, for different network sizes, *N*. (*D*) Critical bond occupation probability, p_c, and the maximum, $\chi_{\max}$, of the susceptibility, χ, as functions of network size, *N*. The dashed lines are power-law fits, and the black symbols in *D* indicate the original network. The GBG and GR shells are produced with $b = 2$.

The fraction of links removed, p, acts as a control parameter that can be manipulated to change the state of the system in in silico experiments, and the transition occurs at some specific value: p_c. Close to this critical point, the macroscopic properties of the network, such as the relative size of the largest connected cluster and the average cluster size, behave as power laws of the distance to the critical point, $(p - p_c)^{\delta}$, with some critical exponents. One way of extracting these exponents is by observing how certain quantities vary as the size of the system changes. However, the finite size scaling technique has faced serious challenges in real networks due to the lack of data beyond single snapshots.

Next, we show that a downward–upward multiscale shell of replicas produced by the joint action of the GBG and GR techniques on a real Internet network (see *SI Appendix*, Fig. S32 for the statistical properties of the replicas as compared with the original network) can be used to study the finite size scaling behavior of bond percolation using only the data from a single snapshot (Fig. 5 *B* and *D*). We measured the average size of the largest component, $\langle G \rangle$, and its fluctuations—i.e., susceptibility $\chi = \frac{\langle G^2 \rangle - \langle G \rangle^2}{\langle G \rangle}$—as a function of p in each layer of the multiscale shell using the fast algorithm of Newman and Ziff (62). In finite systems, a peak in the susceptibility, χ, diverging with the system size indicates the presence of a continuous phase transition, and its position provides a way to estimate the percolation threshold, p_c: Fig. 5*B*. In Fig. 5*D*, we show that the critical link failure probability, p_c, approaches zero as a power law, $p_c(N) \sim N^{-0.374}$, and the maximum, $\chi_{\max}$, of the susceptibility also diverges as a power law: $\chi_{\max}(N) \sim N^{0.456}$. Not only do these results suggest a vanishing percolation threshold in the real Internet graph, as usually happens in scale-free networks, but they also provide a method to estimate the corresponding critical exponents numerically, thus offering a way to study critical phenomena in single-instance real networks.

Conclusions

Real networks are observed to evolve in a self-similar way that preserves their topology throughout the growth process over long time spans. The GBG model lays out a minimal number of simple principles that combine branching growth, one of the paradigms of evolution, and network geometry to explain the empirical findings via a technique that generates self-similar metric expansion of a network replicating its original structure. One of the essential assumptions in the model, the preservation of the distribution of hidden degrees as the number of nodes increases, leads to the introduction of stable distributions in the context of network modeling. Stable distributions, a rich family of probability distributions with intriguing theoretical and practical properties, are widely used to model heavy-tailed data from many types of physical and economic systems and represent an alternative to the power-law paradigm in the study of complex networks. Meanwhile, the GBG model relies on a universal connectivity law that operates at all scales, simultaneously encoding short- and long-range connections, which keeps its form over time. Our results suggest that the same principles organize network connectivity at different length scales in real networks and that these principles are also sustained over time. As a result, simplicity, as one of the rationales for self-similarity, is one of the keys to understanding and predicting network evolution.

While some limitations of our model are obvious—for instance, the exclusion of the birth/death processes of links and nodes—we believe that complementary hypotheses would not affect the results and our GBG model in any fundamental way. The model captures the main mechanisms that drive and predict the self-similar evolution of real networks. In parallel, and beyond the explanatory power of the model to effectively decode the self-similar evolution of real networks, GBG is also a technique to produce scaled-up replicas of networks: an effective and versatile tool facilitating analysis of the behavior of networks at different size scales. The combination of GBG with scaled-down network replicas produced by GR provides full up-and-down self-similar multiscale unfolding of complex networks that covers both large and small scales. Potential applications that require optimization or control of system size in complex systems are countless. Apart from those explained here, we can mention the assessment of scalability issues in dynamic processes in core functions of real networks, such as in Internet routing protocols.

Finally, the presence of symmetry has been observed to affect synchronization on networks (63) and the spectrum of eigenvectors of the Laplacian matrix (64), which controls diffusive processes. Future work will be needed to clarify the influence of the evolutionary self-similarity of real networks described in this paper on dynamical processes taking place on them.

Materials and Methods

Generating $z^{\pm}$. First, we infer the parameters of the stable distribution of a given layer α, η, c, and d. Then, if $b = 2$, meaning that all nodes split, the distribution for descendants,

$$f(z^{\pm}; \alpha^{\pm}, \eta^{\pm}, c^{\pm}, d^{\pm}) = f(z^{\pm}; \alpha, \eta, c/2^{1/\alpha}, d/2), \quad [4]$$

follows immediately from Eq. **2**, and basic properties of the stable distribution, with the shape parameters remaining invariant, and scale and location

being adjusted so that the stable distribution of the ancestor layer is recovered when we sum the hidden variables $z^{\pm}$ of the descendants. These functions and Bayes' rule can be used to generate numerically the values of z^{+} from the probability of hidden degrees of descendants, conditional on the degree of the ancestor $\rho(z^{+}|z)^{\mathrm{nor}}$, normalized to ensure that the hidden degrees of descendants are nonnegative. Finally, once z^{+} has been generated, z^{-} is calculated deterministically by using $z^{-}=z-z^{+}$, and the variables $z^{\pm}$ are transformed back into $\kappa^{\pm}$ using $\kappa=z^{1/\beta}$ (*SI Appendix*, section IV). In the case of fractional b, we produce the hidden variables $z^{\pm}$ of the descendants of branching nodes using $f(z;\alpha,\eta,c/b^{1/\alpha},d/b)$ and assume that the stable distribution in the new layer is $f(z;\alpha,\eta,c/b^{1/\alpha},d/b)$. This gives a good approximation to the mixture of stable distributions that result from nodes with different branching behavior. *SI Appendix*, Fig. S6 demonstrates that the distribution of hidden variables z of descendants has the same shape as that of the ancestor layer in different real networks.

Inflationary GBG. We first proceed as in the noninflationary case. Once we have a noninflationary GBG map, we set $\mu'_a=a\mu'=ab\mu$, $(a\geqslant 1)$ to adjust the average degree to a larger value by adding extra links between any pair of nodes that remained unconnected using probability:

$$\pi_{ij}=\frac{p_{ij}(\mu'_a)-p_{ij}(\mu')}{1-p_{ij}(\mu')}. \qquad [5]$$

These steps ensure that 1) all pairs of descendants in the GBG layer are connected with probability $p_{ij}(\mu'_a)$, with the original form Eq. **1** in the ancestor layer, and hence the resulting network belongs to the $\mathbb{S}^1$ ensemble; 2) links exist between descendants of connected ancestors; and 3) the noninflationary limit is recovered for $a=1$, that is, in this case, $\pi_{ij}=0$, and no extra links are formed so that GBG complies with GR, and there are only connections in the descendant layer between descendants of the same ancestor or of connected ancestors.

Data Availability. Backbones of the WTW were taken from ref. 19. Backbones of the WTW and the JCN and their hyperbolic maps have been deposited in the Zenodo platform and can be freely accessed (https://zenodo.org/record/4023964) (65).

ACKNOWLEDGMENTS. This work was supported by a James S. McDonnell Foundation Scholar Award in Complex Systems; the Catalan Institution for Research and Advanced Studies Academia award, funded by the Generalitat de Catalunya; Agencia Estatal de Investigación Project PID2019-106290GB-C22; Spanish Ministerio de Ciencia, Innovación y Universidades Project FIS2016-76830-C2-2-P (AEI/FEDER, UE); project Mapping Big Data Systems: Embedding Large Complex Networks in Low-Dimensional Hidden Metric Spaces, Ayudas Fundación BBVA a Equipos de Investigación Científica 2017; and Generalitat de Catalunya Grant 2017SGR1064. Furthermore, G.G.-P. was supported by the Academy of Finland via Center of Excellence Program Projects 312058 and 287750; and from the emmy.network foundation under the aegis of the Fondation de Luxembourg.

1. A. Barabási, R. Albert, Emergence of scaling in random networks. *Science* **286**, 509–512 (1999).
2. P. L. Krapivsky, G. J. Rodgers, S. Redner, Degree distributions of growing networks. *Phys. Rev. Lett.* **86**, 5401–5404 (2001).
3. G. Bianconi, A.-L. Barabási, Competition and multiscaling in evolving networks. *Europhys. Lett.* **54**, 436–442 (2001).
4. F. Papadopoulos, M. Kitsak, M. Á. Serrano, M. Boguñá, D. Krioukov, Popularity versus similarity in growing networks. *Nature* **489**, 537 (2012).
5. R. V. Solé, R. Pastor-Satorras, E. Smith, T. B. Kepler, A model of large-scale proteome evolution. *Adv. Complex Syst.* **5**, 43–54 (2002).
6. R. Pastor-Satorras, E. Smith, R. V. Solé, Evolving protein interaction networks through gene duplication. *J. Theor. Biol.* **22**, 199–210 (2003).
7. A. N. Kolmogorov, N. A. Dmitriev, "Branching random processes" in *Selected Works of A. N. Kolmogorov*, A. N. Shiryayev, Ed. (Springer Science+Business Media, Dordrecht, The Netherlands, 1992), pp. 309–314.
8. G. García-Pérez, M. Boguñá, M. Á. Serrano, Multiscale unfolding of real networks by geometric renormalization. *Nat. Phys.* **14**, 583–589 (2018).
9. K. G. Wilson, The renormalization group: Critical phenomena and the Kondo problem. *Rev. Mod. Phys.* **47**, 773 (1975).
10. K. G. Wilson, The renormalization group and critical phenomena. *Rev. Mod. Phys.* **55**, 583 (1983).
11. L. P. Kadanoff, *Statistical Physics: Statics, Dynamics and Renormalization* (World Scientific Publishing Company, Singapore, 2000).
12. C. Song, S. Havlin, H. A. Makse, Origins of fractality in the growth of complex networks. *Nat. Phys.* **2**, 275 (2006).
13. M. Á. Serrano, D. Krioukov, M. Boguñá, Self-similarity of complex networks and hidden metric spaces. *Phys. Rev. Lett.* **100**, 078701 (2008).
14. D. Krioukov, F. Papadopoulos, A. Vahdat, M. Boguñá, Curvature and temperature of complex networks. *Phys. Rev. E* **80**, 035101(R) (2009).
15. G. García-Pérez, M. Á. Serrano, M. Boguñá, Soft communities in similarity space. *J. Stat. Phys.* **173**, 775–782 (2018).
16. K. Zuev, M. Boguná, G. Bianconi, D. Krioukov, Emergence of soft communities from geometric preferential attachment. *Sci. Rep.* **5**, 9421 (2015).
17. D. Hric, K. Kaski, M. Kivelä, Stochastic block model reveals maps of citation patterns and their evolution in time. *J. Inform.* **12**, 757–783 (2018).
18. S. Fortunato *et al.*, Science of science. *Science* **359**, eaao0185 (2018).
19. G. García-Pérez, M. Boguñá, A. Allard, M. Á. Serrano, The hidden hyperbolic geometry of international trade: World trade atlas 1870–2013. *Sci. Rep.* **6**, 33441 (2016).
20. S. Milojević, Quantifying the cognitive extent of science. *J. Inform.* **9**, 962–973 (2015).
21. F. Radicchi, S. Fortunato, C. Castellano, Universality of citation distributions: Toward an objective measure of scientific impact. *Proc. Natl. Acad. Sci. U.S.A.* **105**, 17268–17272 (2008).
22. D. Wang, C. Song, A. Barabási, Quantifying long-term scientific impact. *Science* **342**, 127–132 (2013).
23. Correlates of War Project, State system membership list, v2016. http://correlatesofwar.org. Accessed 18 January 2019.
24. V. D. Blondel, J. L. Guillaume, R. Lambiotte, E. Lefebvre, Fast unfolding of communities in large networks. *J. Stat. Mech. Theor. Exp.* **2008**, P10008 (2008).
25. N. X. Vinh, J. Epps, J. Bailey, Information theoretic measures for clusterings comparison: Variants, properties, normalization and correction for chance. *J. Mach. Learn. Res.* **11**, 2837–2854 (2010).
26. M. Boguñá *et al.*, Network geometry. *Nat. Rev. Phys.* **3**, 114–135 (2021).
27. D. Krioukov, F. Papadopoulos, M. Kitsak, A. Vahdat, M. Boguñá, Hyperbolic geometry of complex networks. *Phys. Rev. E* **82**, 036106 (2010).
28. M. Boguñá, F. Papadopoulos, D. Krioukov, Sustaining the internet with hyperbolic mapping. *Nat. Commun.* **1**, 62 (2010).
29. M. Boguñá, D. Krioukov, P. Almagro, M. Á. Serrano, Small worlds and clustering in spatial networks. *Phys. Rev. Res.* **2**, 023040 (2020).
30. L. Gugelmann, K. Panagiotou, U. Peter. "Random hyperbolic graphs: Degree sequence and clustering," in Automata, Languages, and Programming, A. Czumaj, K. Mehlhorn, A. Pitts, R. Wattenhofer, eds. (Lecture Notes in Computer Science, Springer, Berlin, Germany, 2012), vol. 7392, pp. 573–585.
31. E. Candellero, N. Fountoulakis, Clustering and the hyperbolic geometry of complex networks. *Internet Math.* **12**, 2–53 (2016).
32. M. A. Abdullah, N. Fountoulakis, M. Bode, Typical distances in a geometric model for complex networks *Internet Math.*, 10.24166/im.13.2017 (2017).
33. T. Friedrich, A. Krohmer, On the diameter of hyperbolic random graphs. *SIAM J. Discrete Math.* **32**, 1314–1334 (2018).
34. T. Müller, M. Staps, The diameter of KPKVB random graphs. *Adv. Appl. Probab.* **51**, 358–377 (2019).
35. M. Á. Serrano, D. Krioukov, M. Boguñá, Percolation in self-similar networks. *Phys. Rev. Lett.* **106**, 048701 (2011).
36. N. Fountoulakis, T. Müller, Law of large numbers for the largest component in a hyperbolic model of complex networks. *Ann. Appl. Probab.* **28**, 607–650 (2018).
37. M. Kiwi, D. Mitsche, Spectral gap of random hyperbolic graphs and related parameters. *Ann. Appl. Probab.* **28**, 941–989 (2018).
38. A. Allard, M. Á. Serrano, G. García-Pérez, M. Boguñá, The geometric nature of weights in real complex networks. *Nat. Commun.* **8**, 14103 (2017).
39. K.-K. Kleineberg, M. Boguñá, M. Á Serrano, F. Papadopoulos, Hidden geometric correlations in real multiplex networks. *Nat. Phys.* **12**, 1076–1081 (2016).
40. K.-K. Kleineberg, L. Buzna, F. Papadopoulos, M. Boguñá, M. Á. Serrano, Geometric correlations mitigate the extreme vulnerability of multiplex networks against targeted attacks. *Phys. Rev. Lett.* **118**, 218301 (2017).
41. K.-K. Kleineberg, Metric clusters in evolutionary games on scale-free networks. *Nat. Commun.* **8**, 1–8 (2017).
42. M. Á. Serrano, M. Boguná, F. Sagués, Uncovering the hidden geometry behind metabolic networks. *Mol. Biosyst.* **8**, 843–850 (2012).
43. A. Allard, M. Á. Serrano, Navigable maps of structural brain networks across species. *PLoS Comput. Biol.* **16**, e1007584 (2020).
44. M. Zheng, A. Allard, P. Hagmann, Y. Alemán-Gómez, M. Á. Serrano, Geometric renormalization unravels self-similarity of the multiscale human connectome. *Proc. Natl. Acad. Sci. U.S.A.* **117**, 20244–20253 (2020).
45. G. García-Pérez, A. Allard, M. Á. Serrano, M. Boguñá. Mercator, Uncovering faithful hyperbolic embeddings of complex networks. *New J. Phys.* **21**, 123033 (2019).
46. P. Lévy, *Calcul des Probabilités* (Gauthier-Villars, Paris, France, 1925).
47. S. Borak, W. Härdle, R. Weron. "Stable distributions" in *Statistical Tools for Finance and Insurance*. P. Cizek, W. K. Härdle, R. Weron, eds. (Springer, Berlin, Germany, 2005), pp. 21–44.
48. J. P. Nolan, *Stable Distributions-Models for Heavy Tailed Data* (Springer Nature, Boston, MA, 2019).
49. B. V. Gnedenko, A. N. Kolmogorov, *Limit Distributions for Sums of Independent Random Variables* (Addison-Wesley, Boston, MA, 1954).
50. B. B. Mandelbrot, The variation of certain speculative prices. *J. Bus.* **36**, 394–419 (1963).
51. E. F. Fama, The behavior of stock-market prices. *J. Bus.* **38**, 34–105 (1965).
52. M. Kateregga, S. Mataramvura, D. Taylor, Parameter estimation for stable distributions with application to commodity futures log-returns. *Cogent Econ. Fin.* **5**, 1318813 (2017).

53. J. P. Nolan, Numerical calculation of stable densities and distribution functions. *Commun. Stat. Stoch. Model.* **13**, 759–774 (1997).
54. J. Royuela-del Val, F. Simmross-Wattenberg, C. Alberola-López, libstable: Fast, parallel, and high-precision computation of α-stable distributions in R, C/C++, and MATLAB. *J. Stat. Software*, **78**, i01 (2017).
55. S. N. Dorogovtsev, A. V. Goltsev, J. F. F. Mendes, Critical phenomena in complex networks. *Rev. Mod. Phys.* **80**, 1275 (2008).
56. M. Fire, R. Puzis, Organization mining using online social networks. *Network. Spatial Econ.* **16**, 545–578 (2016).
57. M. Kuperman, D. Zanette, Stochastic resonance in a model of opinion formation on small-world networks. *Euro. Phys. J. B Condens. Matter. Complex Syst.* **26**, 387–391 (2002).
58. L. Gammaitoni, P. Hänggi, P. Jung, F. Marchesoni, Stochastic resonance. *Rev. Mod. Phys.* **70**, 223 (1998).
59. A. Pikovsky, A. Zaikin, M. A. de la Casa, System size resonance in coupled noisy systems and in the Ising model. *Phys. Rev. Lett.* **88**, 050601 (2002).
60. R. Toral, C. J. Tessone, Finite size effects in the dynamics of opinion formation. *Commun. Comput. Phys.* **1**, 1–19 (2006).
61. P. Jung, P. Hänggi, Stochastic nonlinear dynamics modulated by external periodic forces. *Europhys. Lett.* **8**, 505 (1989).
62. M. E. J. Newman, R. M. Ziff, Efficient Monte Carlo algorithm and high-precision results for percolation. *Phys. Rev. Lett.* **85**, 4104 (2000).
63. L. M. Pecora, F. Sorrentino, A. M. Hagerstrom, T. E. Murphy, R. Roy, Cluster synchronization and isolated desynchronization in complex networks with symmetries. *Nat. Commun.* **5**, 4079 (2014).
64. M. T. Schaub, J.-C. Delvenne, R. Lambiotte, M. Barahona, "Structured networks and coarse-grained descriptions: A dynamical perspective" in *Advances in Network Clustering and Blockmodeling*, P. Doreian, V. Batagelj, A. Ferligoj, eds. (John Wiley & Sons, Hoboken, NJ, 2019), pp. 333–361.
65. M. Zheng, G. García-Pérez, M. Boguñá, M. Ángeles Serrano, Scaling up real networks by geometric branching growth. Zenodo. http://doi.org/10.5281/zenodo.4023964. Deposited 11 September 2020.